Analyst

Inkjet-Printed Micro-Calibration Standards for Ultraquantitative Raman Spectral Cytometry

Journal:	*Analyst*
Manuscript ID	AN-ART-03-2019-000500.R1
Article Type:	Paper
Date Submitted by the Author:	26-Apr-2019
Complete List of Authors:	Lalone, Vernon; University of Michigan College of Pharmacy, Pharmaceutical Sciences Fawaz, Maria; University of Michigan College of Pharmacy, Medicinal Chemistry Morales-Mercado, Jomar; Universidad Metropolitana, School of Sciences, Technology, and Environment Mourão, Márcio; University of Michigan, CSCAR Center Snyder, Catherine; University of Michigan College of Engineering, Materials Science and Engineering Kim, Sang; University of Michigan College of Pharmacy, Pharmaceutical Sciences Lieberman, Andrew; University of Michigan Medical Center, Pathology Tuteja, Anish; University of Michigan College of Engineering, Materials Science and Engineering Mehta, Geeta; University of Michigan College of Engineering, Materials Science and Engineering Standiford, Theodore; University of Michigan Medical Center, Pulmonary and Critical Care Medicine Raghavendran, Krishnan; University of Michigan Medical Center, Surgery Shedden, Kerby; University of Michigan, Statistics Schwendeman, Anna; University of Michigan College of Pharmacy, Pharmaceutical Sciences Stringer, Kathleen; University of Michigan Department of Chemistry, Rosania, Gus; University of Michigan College of Pharmacy, Pharmaceutical Sciences

Inkjet-Printed Micro-Calibration Standards for Ultraquantitative Raman Spectral Cytometry

Received 00th January 20xx,
Accepted 00th January 20xx

DOI: 10.1039/x0xx00000x

Vernon LaLone,*[a] Maria V. Fawaz,[b] Jomar Morales-Mercado,[c] Márcio A. Mourão,[d] Catherine S. Snyder,[e] Sang Y. Kim,[a] Andrew P. Lieberman,[f] Anish Tuteja,[e,g] Geeta Mehta,[e,h] Theodore J. Standiford,[i] Krishnan Raghavendran,[j] Kerby Shedden,[d] Anna Schwendeman,[a] Kathleen A. Stringer,[i,k] and Gus R. Rosania*[a]

Herein we report the development of a cytometric analysis platform for measuring the contents of individual cells in absolute (picogram) scales; this study represents the first report of Raman-based quantitation of the absolute mass – or the total amount – of multiple endogenous biomolecules within single-cells. To enable ultraquantitative calibration, we engineered single-cell-sized micro-calibration standards of known composition by inkjet-printer deposition of biomolecular components in microarrays across the surface of silicon chips. We demonstrate clinical feasibility by characterizing the compositional phenotype of human skin fibroblast and porcine alveolar macrophage cell populations in the respective contexts of Niemann-Pick disease and drug-induced phospholipidosis: two types of lipid storage disorders. We envision this microanalytical platform as the foundation for many future biomedical applications, ranging from diagnostic assays to pathological analysis to advanced pharmaco/toxicokinetic research studies.

Introduction

Single-cell analytical technologies have transformed modern biomedical sciences by providing researchers an avenue through which to explore subcellular phenomena and characterize cell population heterogeneity. Over the past decade these techniques have seen rapid development due to rising awareness of the significance of cell population diversity and the pathophysiological consequences of cell subpopulations that play crucial roles in different disease states.[1] Lipid storage diseases, either inherited (e.g. Niemann-Pick disease) or acquired (e.g. drug-induced phospholipidosis, atherosclerosis), manifest as the inappropriate accumulation of lipids and other small molecules within various cells of the body; many of these disorders are poorly understood and notoriously challenging to diagnose.[2-6] As such, a cytometric approach to measure the absolute amount of cellular material and bioaccumulating contents within single cells – herein referred to as "ultraquantitation" – would provide valuable insight into the mechanisms of storage disorder pathogenesis at the single-cell level where it occurs, with foreseeable application as a diagnostic tool in the clinical setting.

Since the first reported Raman microanalysis of eukaryotic cells in 1990, technological innovation has facilitated the evolution of Raman microscopes into powerful analytical tools with incredible potential in the biomedical sciences.[7-13] Raman microscopy enables the chemical analysis of single-cells with submicron resolution.[14-18] In short, an excitation laser induces molecular vibrations in the sample which scatter light across a multitude of wavelengths; the scattered lights are collected and directed across a Charge-Coupled Device (CCD) and the number of photons at each wavelength are converted to electrical signals (i.e. CCD counts), generating Raman spectra which serve as molecular fingerprints that can be interpreted to determine the chemical composition of the sample. Although there are a multitude of reliable reports on Raman-based "absolute" quantitation at the single-cell level, these studies utilize approaches which are limited to estimates of single-cell content from population measurements (e.g. 0.1mg protein/10^6 cells equates to 100pg protein/cell)[19, 20] or to absolute concentration measurements of multiple biomolecules within specific subcellular compartments (e.g. mg/mL protein, lipid, RNA, and DNA within mitochondria, nucleus, etc.).[18, 21] While these studies report on "absolute" measurements in single-cells, the population average and intracellular concentration measurements are inadequate to answer our long-term research question: how much total material is present in each individual cell? Is there a single cell population or multiple, distinct cell populations in the sample? While population average and subcellular concentration measurements certainly provide valuable insight, there are a number of cytometric phenomena that could go unnoticed because of the significant heterogeneity of cell populations. As it specifically relates to the phenotypic analysis of cellular lipid content, the major advantages of our ultraquantitative absolute measurements of total cellular composition are the ability to quantitatively identify "foamy" lipid-laden outlier cells within a population (whereas the influence of lipid-laden outlier cells is diminished through population average measurements of lipid content) and to quantitatively characterize the distribution of compositional phenotypes throughout a cell population (i.e. two cells might have equivalent intracellular concentrations of lipid but one is much bigger and therefore carries a greater total quantity of cargo). We are herein expanding upon the quantitative aspects of previous approaches such as these to make absolute measurements of the total amount of biomolecular material present inside individual eukaryotic cells.

[a] Department of Pharmaceutical Sciences, College of Pharmacy, University of Michigan, Ann Arbor, MI 48109 (USA). Email: grosania@umich.edu; Tel: 734-763-1032
[b] Department of Medicinal Chemistry, College of Pharmacy, University of Michigan, Ann Arbor, MI 48109 (USA).
[c] School of Sciences, Technology, and Environment, Universidad Metropolitana, San Juan, PR.
[d] CSCAR Center, University of Michigan, Ann Arbor, MI 48109 (USA).
[e] Department of Materials Science and Engineering, College of Engineering, University of Michigan, Ann Arbor, MI 48109 (USA).
[f] Department of Pathology, University of Michigan Medical Center, Ann Arbor, MI 48109 (USA).
[g] Biointerfaces Institute, Macromolecular Science and Engineering, Department of Chemical Engineering, University of Michigan, Ann Arbor, MI 48109 (USA).
[h] Department of Biomedical Engineering, Macromolecular Science and Engineering, University of Michigan, Ann Arbor, MI 48109 (USA).
[i] Division of Pulmonary and Critical Care Medicine, Department of Internal Medicine, University of Michigan Medical Center, Ann Arbor, MI 48109 (USA).
[j] Department of Surgery, Michigan Medicine, University of Michigan Medical Center, Ann Arbor, MI 48109 (USA).
[k] Department of Clinical Pharmacy, College of Pharmacy, University of Michigan, Ann Arbor, MI 48109 (USA).

†Electronic Supplementary Information (ESI) available.
See DOI: 10.1039/x0xx00000x

Although the Raman bioanalytical field has blossomed over the past three decades, with substantial advancements in overall instrument performance and a multitude of commercial instruments now available on the market, a standardized quantitative calibration technology for the absolute simultaneous measurement of total biomolecular contents in single cells has yet to be firmly established; as such, we herein propose a Raman analytical methodology for the simultaneous measurement of each major biomolecular components present within single cells using a novel quantitative calibration technology.[22] Our methodology's theoretical foundation was inspired by two separate Raman-based studies of eukaryotic cells: the first measured the absolute amount of a single analyte, glycogen, inside human embryonic stem cells using thin layers of pure glycogen as calibration standards while the second verified integrated area scans over the entirety of individual cells as the optimal Raman acquisition parameters for robust single cell classification.[23, 24] Harmonizing the theoretical concepts from these two studies elucidated the feasibility of simultaneous absolute quantitation of the total amount of each major biomolecular component within individual eukaryotic cells, namely protein, lipid, carbohydrate, and nucleic acid.

Through extensive multidisciplinary collaboration, we fabricated cell-sized micro-calibration standards of known mass and composition using inkjet printing technology with custom biomolecular ink formulations. We utilized synthetic high-density lipoprotein nanodiscs (HDLs) to overcome solubility barrier and dissolve known amounts phospholipid in aqueous ink formulations. Using an inkjet materials printer, 10pL ink droplets were deposited in microarray patterns across the surface of silicon chips; the water from the aqueous-based ink formulations quickly evaporated, depositing the non-volatile biomolecular components as thin dry dispersions across the surface of silicon chips; for example, a 10pL droplet of a 100mg/mL albumin ink solution would contain in total 1000pg of protein that would be deposited as water evaporated. Using the established method for cell sample preparation,[16] eukaryotic cells were allowed to adhere to the surface of silicon chips before brief washing and air-drying to form thin dispersions on the surface of silicon chips. The thin-film interference of light passing through the sample and reflecting off the silicon surface led to a rainbow-colored appearance of cell samples and suggested that the height of dry cell dispersions was typically less than 1µm. To confirm, we measured the topography of air-dried cell dispersions on silicon using atomic force microscopy. Similarly, we confirmed that the height and area of the inkjet-printed, micro-calibration standards was similar to the height and area of the cell samples of interest.

For the acquisition of Raman data, we employed a continuous area scan methodology where the excitation laser scans across the entirety of a given sample, collecting individual spectra at each pixel of the analyzed area; because the height of the 532nm laser confocal voxel (~1.5µm) exceeded the height of our micro-calibration and cell samples, the total mass of each sample could be analyzed in a single-plane Raman area scan. When analyzed with equivalent acquisition parameters, Raman data acquired from the biomolecular micro-calibration standards could be used to quantitatively interpret Raman data acquired from cells of interest. Because each micro-calibration standard contained a known total mass of material, the total (or "integrated") Raman signal acquired from that standard can be used to define the signal-to-mass ratio (i.e. CCD counts/picogram) for the acquisition methodology. Using linear combination modelling with quantitatively-calibrated pure component reference spectra, the integrated Raman spectrum from a single cell (CCD counts) could thereby be deconvoluted into the total mass of each component of interest present within that cell (picograms of protein, lipid, nucleic acid, etc.).

This approach enabled quantitative phenotypic characterization of cell populations – universally applicable to multiple cell types and species – on the basis of absolute biomolecular composition, specifically measuring the total amounts of protein, lipid, nucleic acid and carbohydrate present inside individual eukaryotic cells. It should be noted that the proposed calibration technique is currently limited to dried cells because the micro-calibration standards are fabricated as dry dispersions, though rehydration has not yet been tested; conveniently, this apparent methodological shortcoming actually harmonizes well with our long-term goal of clinical sample analysis where cell samples are commonly prepared as dry dispersions on substrates via cytocentrifugation. Ultimately, the development of robust quantitative micro-calibration standards for Raman instruments will facilitate interlaboratory comparisons of Raman-based cell analyses and contribute to the harmonious advancement of Ramanomics disciplines at the global level.[14] We have termed our novel approach ultraquantitative Raman spectral cytometry and believe it represents a significant advancement in the field of Raman-based biomedical applications.

Materials and methods

Materials

Silicon chips (5x5mm; Ted Pella, Inc., Redding, CA) served as substrates for all Raman measurements performed herein. The following reagents were used to generate the reference spectra library: bovine albumin (MP Biomedicals; Solon, OH), 1,2-dipalmitoyl-sn-glycero-3-phosphocholine (DPPC; Avanti Polar Lipids, Inc., Alabaster, AL), 1,2-dioleoyl-sn¬-glycero-3-phsophocholine (DOPC; Avanti Polar Lipids, Inc., Alabaster, AL), DNA (from salmon sperm; AmResco Inc., Solon, OH), and cholesterol (ovine; Avanti Polar Lipid, Inc., Alabaster, AL). Polysorbate 20 (Bio-Rad Laboratories, Inc., Hercules, CA) was utilized as surfactant in diluent for albumin ink formulations. The following reagents were used to formulate HDL nanoparticle suspensions: 22A (PVLDLFRELLNELLEALKQKLK) was synthesized by Genscript (Piscataway, NJ), using solid-phase Fmoc (9-fluorenylmethyl carbamate) chemistry and purified with reverse phase chromatography (>95 % pure). 1,2-dipalmitoyl-sn-glycero-3-phosphocholine (DPPC) was purchased from NOF America Corporation and cholesterol was obtained from Sigma-Aldrich (St. Louis, MO).

Preparation and characterization of synthetic high-density lipoproteins

Synthetic high-density lipoproteins (HDL) composed of 22A peptide and DPPC was prepared by a co-lyophilization procedure (Di Bartolo et al., 2011). Briefly, peptide and phospholipid were dissolved in glacial acetic acid, mixed at 1:2 wt/wt ratio, and lyophilized overnight. The powder was rehydrated with water to make 30 mg/mL (based on peptide concentration) HDL and thermocycled between 55° C (10 min) and room temperature (10 min) thrice to facilitate HDL formation. HDL containing cholesterol was prepared using a thin film method (Tang et al., 2017). DPPC and cholesterol (10:1 wt/wt) were dissolved in chloroform and 22A was dissolved in water/methanol (3:4 v/v) solvents. Then, lipid and peptide solutions were combined at 1:2 (wt/wt) 22A-to-DPPC ratio, sonicated for 1 min at room temperature, and solvents evaporated under the stream of N2 gas to form a thin film. Lastly, the film was rehydrated in water for a final 90 mg/mL concentration (60mg/mL lipid and 30mg/mL peptide 22A) and then probe sonicated for 2 min at 4W with 10 sec pulses to form HDL containing cholesterol. The resulting HDL

complexes were diluted to 1 mg/mL (based on peptide concentration) with water and analyzed by gel permeation chromatography (GPC) for purity using 7.8 mm x 30 cm Tosoh TSK gel G3000SWxl column (Tosoh Bioscience, King of Prussia, PA) with 1 mL/min flow rate (PBS pH 7.4). Free peptide and HDL peaks were detected at 220 nm. The HDL hydrodynamic diameters were determined in water at 1 mg/mL by dynamic light scattering (DLS) using a Zetasizer Nano ZSP, Malvern Instruments (Westborough, MA). The volume intensity average values (± SD) were reported. Nanoparticle size and morphology were verified using transmission electron microscopy.

Aqueous printer ink formulations

All fluidic printer inks were formulated as aqueous solutions and/or nanoparticulate suspensions in HPLC-grade water. To ensure accurate and precise performance of different ink solutions, each was formulated to achieve the following fluid property specifications: viscosity within the ranges of 0.010 to 0.012 Pa*s at 25°C, surface tension within the range of 28-33 mN/m, a maximum suspended particle size of 200nm or less, and the absence of dissolved gas. A stock solution of 100mg/mL albumin was formulated in diluent (0.25% polysorbate 20 in HPLC-grade water) to reduce surface tension between 28 and 33 dynes/cm and achieve viscosity between 0.010 and 0.012 Pa*s; in this way, a 10pL drop would theoretically contain 1000pg of protein with negligible surfactant content (<0.5% wt/wt). Additional albumin inks were formulated by serial dilutions of albumin stock with diluent to generate 500pg, 250pg, and 100pg protein micro-calibration standards. By formulating aqueous printer inks with (synthetic) high density lipoprotein particles (stock solution containing 90mg/mL HDL in water), we were able to use the inkjet printer to fabricate calibration dot microarrays with known amount of total phospholipid present. Multi-component calibration mixtures were created by stoichiometric mixtures of albumin stock solution with HDL or HDL+cholesterol stock solutions; by varying the concentrations of protein and HDL particles and incorporating cholesterol, we fabricated mixed composition micro-calibration standards of three unique compositions: 1) 350pg protein/peptide, 200pg lipids, and 20pg cholesterol; 2) 575pg protein/peptide, 150pg lipids, and 0pg cholesterol; 3) 550pg protein/peptide, 100pg lipids, and 10pg cholesterol.

Piezoelectric inkjet printing of microarrays

Approximately 1.5mL of each fluidic printer ink was first de-gassed via sonication and filtered through a 0.22µm filter directly into separate printer cartridges (10pL drop volumes). A Dimatix MP-2831 piezoelectric inkjet materials printer (FUJIFILM Dimatix, Inc., Santa Clara, CA) equipped with specific cartridge fluid modules and piezoelectric inkjet nozzles, was used to deposit droplets of 10 picoliter (pL) volumes with tailor-made ink formulations in a defined array pattern across the surface of silicon chips. Printing parameters, specifically the piezoelectric jetting waveform shown in Scheme 1b and the nozzle temperature set to 35°C, were used to enable successful deposition of each fluid across the surface of the silicon chips as microarrays. We printed these droplets on to 5mm x 5mm silicon wafer chips that are well-suited for Raman spectral imaging, as they possess a low and constant background signal that can be subtracted out from the cellular signal. The droplets are air dried directly on the chip in approximately 1 minute with a substrate temperature of 40°C and atmospheric pressure (1 atm) and are visible as brightly colored spots under reflected light illumination.

Atomic force microscopy

Topographical images of micro-calibration standards and fibroblast preparations on silicon chips were obtained using a Bruker Innova AFM with TESPA probes in tapping mode to measure the height across the area of each sample of interest. The data in each image was plane-fit to establish a level background of the silicon substrate and height data at each image pixel was used to generate pseudo-color topographical maps for each sample analyzed using NanoScope Analysis v1.6.

Raman measurements

All Raman measurements were recorded using a WITec alpha300 R Confocal Raman Imaging Microscope (Ulm, Germany) equipped with a 50X air objective lens (Zeiss EC EPIPLAN, N.A.=0.75) and 532nm solid-state excitation laser (0-55mW, tunable intensity range with attenuator dial) coupled to a CCD detector via a 100µm diameter multi-mode fiber-optic cable. Raman area scans were performed by first locating the optimal laser focal plane for sample excitation (yielding the greatest signal intensity from 2800-3100cm^{-1} for biological materials) then continuously acquiring data across that area of interest by scanning in raster pattern, presumably exciting the entirety of the sample material present. The excitation laser intensity was kept constant between sample scans. Fibroblast cell datasets and corresponding calibration micro-calibration standard datasets were acquired via 60x60µm area scans and step-size of 1µm (3600 spectra/pixels) with an integration time of 0.05 sec per pixel, for an acquisition time of 3 min per cell (or micro-calibration standard). Alveolar macrophage cell datasets and corresponding micro-calibration standard datasets were acquired via 25x25µm area scans with a step-size of 1µm (625 spectra/pixels) with an integration time of 0.1 sec per pixel, for an acquisition time of 1 min per cell (or micro-calibration standard). By continuously acquiring Raman signal data in a raster pattern across the scan area at the optimal focal plane, hyperspectral Raman datasets were generated which were presumably representative of the entirety of each sample that was analyzed. 40 fibroblast cells from each group (WT and NPC) and 35 macrophages from each group (control and drug-treated) were analyzed herein; each cell was scanned once.

Spectral preprocessing and hyperspectral image processing

All acquired Raman spectra underwent equivalent preprocessing procedures; cosmic ray removal (filter size: 4; dynamic factor: 4.6) is performed on a per-pixel basis in WITec Project FOUR software before data is exported to Matlab® (Mathworks, Inc., Natick, MA) where remainder of preprocessing is executed via an algorithm developed in-house. Spectral background subtraction was performed by regression fitting of baseline estimation throughout multiple shifted windows across the integrated spectrum via spline approximation. Throughout this work, two different types of pseudo-colored images were generated from Raman area scan datasets: "single-band" images and "multi-band" images. Single-band images were generated by selecting a single Raman band (the Raman intensity at a single wavenumber), specifically 2930cm^{-1}, and converting the intensity (CCD counts) at each pixel across the image into a color. Multi-band images were generated by separately calculating the "lipid signal" (sum of spectral intensities from 2800-2900cm^{-1}, assigned to green channel; pixel intensity range displayed from 0-500 CCD counts) and the "protein signal" (sum of spectral intensities from 2905-2935cm^{-1}, assigned to red channel; pixel intensity range displayed from 0-500 CCD counts), and then overlaying the two images. To calculate the "integrated Raman intensity" for each area scan (of a single cell or micro-calibration standard), all pixel spectra are added together to generate a single "integrated" spectrum which is

representative of the composition and total amount of material present within the given area scan. The spectral region of interest (2700-3200cm-1) was excised from the integrated spectrum and interpreted via statistical models discussed in the following sections.

Statistical Model for Ultraquantitative Spectral Deconvolution

To generate reference spectra, biomolecular components of interest were dissolved in appropriate solvent at ~1mg/mL (DI water for protein and nucleic acid; methanol for lipids and cholesterol) and spotted onto the surface of silicon chips; the solvent evaporated at room temperature, depositing all non-volatile solutes across the surface of silicon chips. Reference spectra were acquired via continuous large area scans of each dried dispersion and the average spectrum across each scan was extracted, thereby generating "molecular fingerprints" for each biochemical component of interest. Using Raman datasets acquired from protein and HDL calibration microarrays, the pure component reference spectra were scaled accordingly to directly relate the total mass of each component present within an analyzed microarray dot to the integrated Raman signal acquired from across that region (i.e. CCD counts / picogram). Measured Raman spectra were deconvoluted via linear combination modelling (aka: non-negative least squares regression modelling) with the ultraquantitative reference spectra as per the following equation:

$$\boldsymbol{I_{\tilde{\nu}} = N_1 k_{\tilde{\nu}_1} + N_2 k_{\tilde{\nu}_2} + N_3 k_{\tilde{\nu}_3} + N_4 k_{\tilde{\nu}_4} + \varepsilon_{\tilde{\nu}}}$$

Where:

$\boldsymbol{I_{\tilde{\nu}}}$ = integrated sample spectrum (CCD counts)

$\boldsymbol{k_{\tilde{\nu}_n}}$ = "n" reference spectrum (CCD counts / picogram)

$\boldsymbol{N_n}$ = "n" measurement (picograms)

$\boldsymbol{\varepsilon_{\tilde{\nu}}}$ = residual spectrum (CCD counts)

$\boldsymbol{\tilde{\nu}}$ = relative wavenumber or Raman shift (cm^{-1})

$\boldsymbol{n}$ = biomolecular component (e.g. protein, lipid, etc.)

The linear combination spectral model accuracy of fit was assessed by calculating coefficient of determination (R^2) for each micro-calibration standard spectrum fit according to the following equation:

$$\boldsymbol{Spectral\ model\ fit\ (R^2) = 1 - \left(\frac{variance(\varepsilon_{\tilde{\nu}})}{variance(I_{\tilde{\nu}})}\right)}$$

We refer to this approach as "ultraquantitative" spectral deconvolution; it conveniently yields regression estimate coefficients with units of picograms because it harmonizes effectively with the fundamental theory of linear spectroscopy.

Additional statistical models for interpretation of cytometric data

Principal component analysis (PCA) was also performed on integrated Raman spectra; standard normal variate scaling was performed on each integrated spectrum prior to PCA execution in Matlab®. Logistic regression analysis of ultraquantitative results (picogram measurements) from cell datasets and K-means cluster analysis of PCA results (PC scores) were both performed in R Studio using scripts written in-house; logistic regression model was performed as per the following equations:

$$\boldsymbol{Population \sim Protein + Lipid + Cholesterol + Carbohydrate \,\&\, Nucleic\ Acid}$$

(for fibroblast dataset)

and

$$\boldsymbol{Population \sim Protein + Lipid + Carbohydrate \,\&\, Nucleic\ Acid}$$

(for macrophage dataset)

Instrument calibration check procedure and error analysis

A novel Raman instrument calibration and daily check was developed to assess instrument performance and drift and quantitatively correct for any errors that may be inadvertently introduced as a result of extraneous factors. Conveniently, the silicon chip substrates served as calibration standards for detector alignment (using major silicon peak at 521cm-1). The optimal focal plane can be located (z-plane of greatest Raman signal at a given laser intensity) and by varying the intensity of excitation laser across a range of 0-55mW, acquiring Raman spectra at given intervals, enabled generation of instrument performance curves which were indicative of the instrument's performance.

Sample preparation of primary human fibroblasts

Primary human fibroblast cell lines were obtained from the NIGMS Human Cell Repository at the Coriell Institute for Medical Research. A control (WT) cell line GM08399 and NPC cell line with mutations in the NPC1 gene GM18453 (I1061T/I1061T) were cultured in DMEM, 1% penicillin/streptomycin, and 10% FBS. Cells were suspended in culture medium containing 10% FBS at a concentration of 10,000 cells/mL. 5x5mm silicon chips were pre-sterilized and transferred to wells of 24-well plate before addition of 1 mL of each cell suspension to separate wells. The plates were incubated overnight (37°C, 5% CO_2) to allow cells to adhere to surface of substrate. Following incubation, culture medium was removed by vacuum and silicon chips were rinsed via brief submersion in isotonic saline (0.9% NaCl wt/wt) the deionized water to remove excess salt; residual water was wicked away immediately with a KimWipe to prevent cell lysis. This methodology prepared cell samples as thin dry dispersions of non-volatile biomolecular components deposited onto the surface of silicon chip substrates.

Animal Protocol and Ethics

Animal experiments were performed according to the University of Michigan's Institutional Animal Care and Use Committee-approved protocol (PRO00008551). All animal procedures were performed in accordance with the Guidelines for Care and Use of Laboratory Animals of the University of Michigan and approved by the Animal Ethics Committee of the University of Michigan.

Isolation, incubation, and preparation of porcine macrophages

Porcine alveolar macrophages were isolated via bronchoalveolar lavage with 40mL instillation of isotonic saline (0.9% NaCl wt/wt) into the lung of a fully-anesthetized male pig (Michigan State Swine Research; *Sus scrofa domesticus*; Yorkshire/Yorkshire mix; ~13-15 weeks old). The acquired cell suspension was diluted to 500,000 cells/mL in RPMI medium 1640, 5% FBS, and 1% penicillin/streptomycin. 15µL aliquots were seeded onto 5x5mm silicon chip substrates in a 24-well plate, allowed to adhere to substrate surface (60 minutes, 37°C, 5% CO_2), before wells were filled to 750µL with blank control medium or treatment medium containing 8µM amiodarone, a widely used antiarrhythmic known to accumulate in alveolar macrophages and induce intracellular accumulation of phospholipids. Treatment

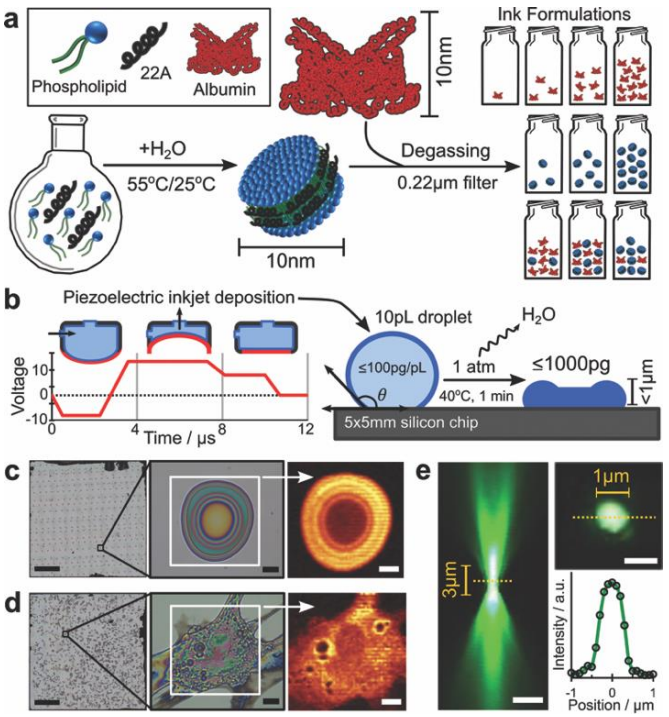

Scheme 1. (a) Procedure for HDL synthesis and biomolecular ink formulations. (b) Piezoelectric jetting waveform for controlled-deposition of 10pL ink droplets onto silicon substrate. Reflected brightfield images of 5x5mm silicon chips (scale bars: 1000μm) and sample areas of interest with corresponding Raman area scan (white box; scale bars: 10μm) data for (c) fabricated micro-calibration standards and (d) fibroblasts. Raman images reconstructed from C-H vibration intensity at 2930cm^{-1}. (e) Vertical cross-section of confocal voxel; reflected light image stack was used to reconstruct in 3D. Scale bars: 3μm (left) and 1μm (right).

populations were incubated for 3 days (37°C, 5% CO_2), replacing medium every 24 hours, to allow cells to sequester drug and induce intracellular accumulation of phospholipids. Following incubation, culture medium was removed by vacuum and silicon chips were rinsed via brief submersion in isotonic saline (0.9% NaCl wt/wt) then deionized water to remove excess salt; residual water was wicked away immediately with a KimWipe to prevent cell lysis. This methodology prepared cell samples as thin dry dispersions of non-volatile biomolecular components deposited onto the surface of silicon chip substrates.

Results and discussion

Engineering solutions to biophysical barriers of cell-sized biomolecular calibration standard fabrication

The first step was engineering and fabrication of cell-sized calibration standards. Microarrays have previously been generated with DNA, RNA, protein, and pharmacological agents for use in biosensors, immunoassays, and high throughput screening procedures for identification of drug candidates.[25-28] Using a piezoelectric inkjet materials printer to deposit 10pL ink droplets in microarrays across the surface of silicon chips, we successfully fabricated cell-sized micro-calibration standards of known composition; printer inks were formulated as aqueous solutions of analytes at biologically-relevant concentrations (Scheme 1a). As residual water evaporated from the droplets, a known mass of dry material was deposited onto surface of the chip (Scheme 1b). Ink solutions were formulated with analytes of interest in concentrations ranging from 0-100mg/mL (equivalent to 0-100pg/pL), yielding calibration standards across a mass range of 0-1000pg when depositing ink volume of 10pL. The fabrication of water-soluble analyte microarrays, namely protein, was achieved with ink concentrations of albumin up to 100mg/mL. Synthetic high-density lipoprotein (HDL) nanodiscs were utilized to overcome the barrier of low lipid solubility in aqueous solution and to achieve proper fluid properties.[29-31]

HDL nanodiscs were synthesized as stoichiometric mixtures of phospholipid (1,2-dipalmitoyl-sn-glycero-3-phosphocholine, DPPC) and biomimetic peptide 22A (2:1 mass ratio) via thermocycling method to achieve up to 90mg/mL HDL in water.[32] Characterization of HDLs revealed an average particle diameter of 10nm (Figure S1).[33-35] We demonstrated the ability to print micro-calibration standards across a total lipid range of 0-600pg; at 90mg/mL HDL, a 10pL ink droplet contained 600pg of lipid and 300pg of peptide for a total mass of 900pg. HDLs allowed for incorporation of known amounts of lipophilic analytes (i.e. cholesterol) and proved miscible with albumin in lipid-to-protein ratios expected to occur in living cells, enabling fabrication of biologically-relevant cell-sized micro-calibration standards of mixed composition.[36]

Cell samples of interest were prepared, according to a method previously developed by our group, on silicon chips as thin dry dispersions, nearly equivalent to the state of the micro-calibration standards, and analyzed by atomic force microscopy (AFM) and Raman microscopy, exploiting the non-destructive nature of both techniques (Scheme 1c, d).[16] Reflected brightfield imaging revealed similar appearance for micro-calibration standards and cell samples of interest (Figure 1a-c). AFM analysis enabled comparison of topographical morphology between micro-calibration standards and cell samples (Figure 1d-f, S2-4). Micro-calibration standards were found to have diameters and height ranges of the same order as cells and yielded comparable Raman signals (Figure S5). All maximum sample heights, actual cells and micro-calibration standards, were in the submicron range and found to be shorter than the height of the Raman excitation laser's confocal voxel (Scheme 1e), suggesting the entirety of each sample may be analyzed in a single x-y plane area scan.[23, 37] Raman area scans revealed the density and distribution of molecular components throughout each analysis region, illustrating how thicker sample regions with presumably greater amounts of material yield stronger Raman signals compared to thinner regions with less total material (Figure 1g-I, S6-15).

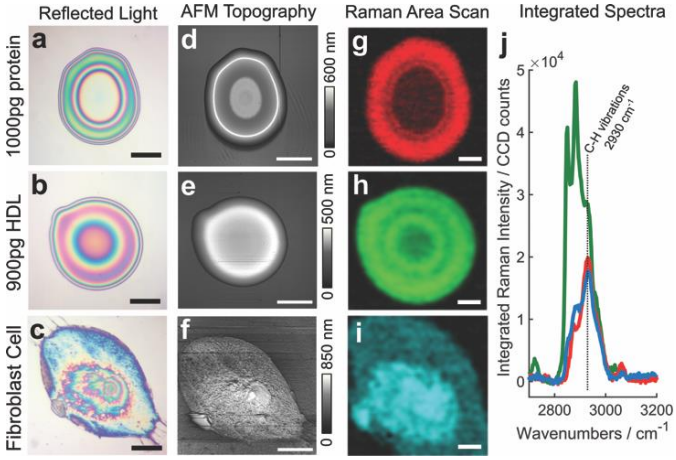

Figure 1. Reflected light images of 1000pg protein (a), 900pg HDL (b), and fibroblast (c) samples; scale bars: 20μm. Respective AFM surface profiles (d-f); scale bars: 20μm. Respective single-band Raman images reconstructed from C-H vibrations at 2930cm^{-1} (g-i) and calculated integrated Raman spectra for each overlaid on same y-axis (j); scale bars: 10μm.

Integrated Raman spectra were calculated from the total Raman signal across each analysis area, yielding a single spectrum for each sample that is representative of the total molecular content present within the area scan; a greater integrated Raman intensity was acquired from 900pg of HDL than from 1000pg of protein, suggesting different analytes of interest emit different Raman signal strengths under the same excitation parameters.

Although 633nm and 785nm lasers are generally used for Raman analysis of biological cells, in this study we utilized a 532nm excitation laser because the visible green light enabled facile characterization of the confocal voxel dimensions and yielded the strongest Raman signals from our samples, and thus allowed measuring the smallest amounts of material. During preliminary feasibility testing, we also fabricated microarrays on glass slides and prepared macrophages via cytocentrifugation on glass slides (Figure S16). Alternative sample substrates (e.g. CaF2) could be compatible with inkjet-printed micro-calibration standards, to the extent that the samples yield strong Raman signals, and that the background Raman signals from the substratum can be subtracted. Instrument performance curves suggested instrument-introduced errors were present but negligible; further work is needed in advancement of Raman instruments to ensure measurement accuracy, which our calibration micro-calibration standards will help facilitate (Figure S17). From preliminary experiments, we have verified the performance of each individual inkjet cartridge nozzle exhibits excellent drop-to-drop consistency, generating droplet rows which show minimal measurement variability, ~5%, while different nozzles within the same cartridge show a greater variation in drop size, leading to columns measuring somewhat greater variability, ~10-15% (Figure S18).

Microarrays and the linearity of scattered Raman signals

Micro-calibration standards were composed of proteins and lipids in ratios and total mass ranges consistent with theoretical estimates for typical eukaryotic cells, thereby demonstrating the feasibility of commercially-available piezoelectric inkjet printing technology for creation of mimic cells; using constant experimental parameters, the integrated Raman signals were acquired from areas of interest for a multitude of micro-calibration standards from each group (Figure 2a-g). Using linear combination modelling, pure component reference spectra were scaled to optimize fit of entire micro-calibration standard dataset, thereby building a quantitative spectral library which directly related the acquired CCD counts to picograms for each component (Figure 2h). Linear combination spectral modelling yielded reliably accurate fits which were assessed by coefficient of determination (R^2) for each micro-calibration standard spectrum fit; R^2 values were greater than 0.975 for all samples with the exception of the 100pg protein micro-calibration standards (attributable to lower signal-to-noise ratio of the integrated spectra acquired from lesser sample mass), verifying the accuracy of integrated sample spectral fit using pure component reference spectra (Figure 2i). Protein, lipid, and protein-to-lipid ratio measurements for all micro-calibration standards showed strong correlation with the expected values, revealing the linearity of integrated Raman signals in relation to the absolute mass of each material present within the scanned area of interest and suggesting supramolecular interactions between biological analytes do not interfere with the linearity of the scattered Raman signals (Figure 2j-l, S19-21).[38]

High-content phenotypic analysis of cell populations

To show proof-of-concept for our methodology and establish validity for cytometric applications, human skin fibroblast populations - wild type

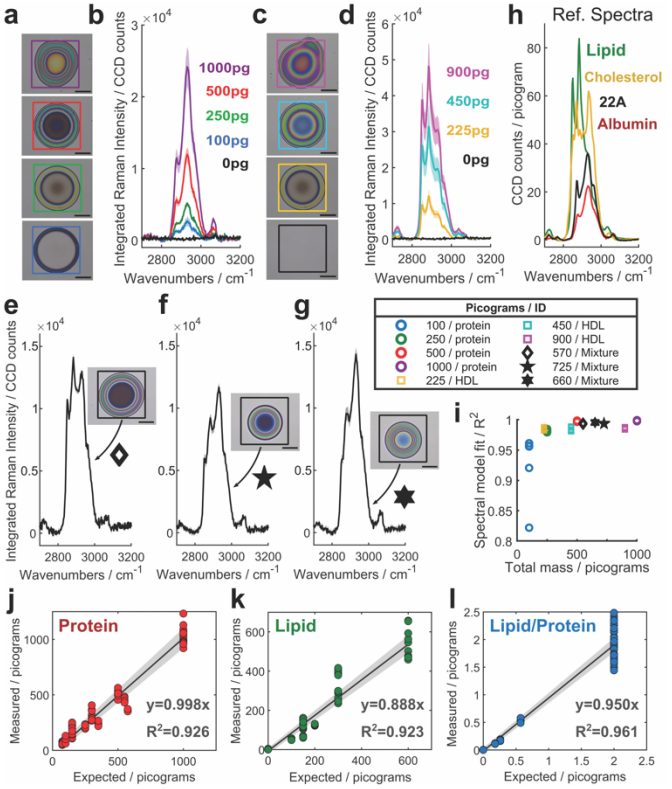

Figure 2. Reflected brightfield images, analysis areas and corresponding integrated spectra for (a-b) protein, (c-d) HDL, and (e-g) mixed composition micro-calibration standards; scale bars: 20µm. (h) Reference spectra library for linear combination modelling. (i) Accuracy of spectral fits. Linear regression of measured component content in relation to expected amount for protein (j), lipid (k), and lipid-to-protein ratio (l); shaded regions: 95% confidence interval.

(WT) and Niemann-Pick Type C (NPC) – and porcine alveolar macrophages – untreated and drug-treated groups - were prepared as dry dispersions on the surface of silicon chips, closely resembling the micro-calibration standards; a small number of cells from each population were analyzed (Figure 3a). It is worth noting that this sample preparation technique may be applied to non-adherent cell types through conventional cytocentrifugation to deposit and dry suspended cells onto silicon chip substrates; in this way alternative substrates could be utilized (i.e. CaF_2, glass slides, etc.) for cell preparation, depending on substrate chosen for micro-calibration standard printing or other experimental needs (Figure S16). Raman images of single cells revealed the subcellular distribution of protein (red channel) and lipid (green channel), enabling clear distinction between nuclei and cytoplasm (Figure 3b). Furthermore, Raman imaging revealed lipid-rich inclusions (presumably lamellar bodies) in alveolar macrophages treated with 8µM amiodarone, a lipophilic weakly basic drug that induces phospholipidosis, an adverse drug reaction characterized by a lipid-laden macrophage phenotype (Figure 3c, S22).[5, 6, 39, 40] Stoichiometric mixtures of protein and DNA were used to estimate relative Raman signal strength of carbohydrates and nucleic acids (Figure S23); in future validation work, additional biomolecular components (e.g. DNA, RNA, polysaccharides, cytochrome c, etc.) will be incorporated into artificial cell mimic micro-calibration standards. Using our quantitatively-calibrated reference spectra library to perform linear combination modelling (Figure 3d), integrated cell spectra were deconvoluted, thereby yielding measurements for total picograms of each biomolecular component present within each cell analyzed. The high variability of our cytometric

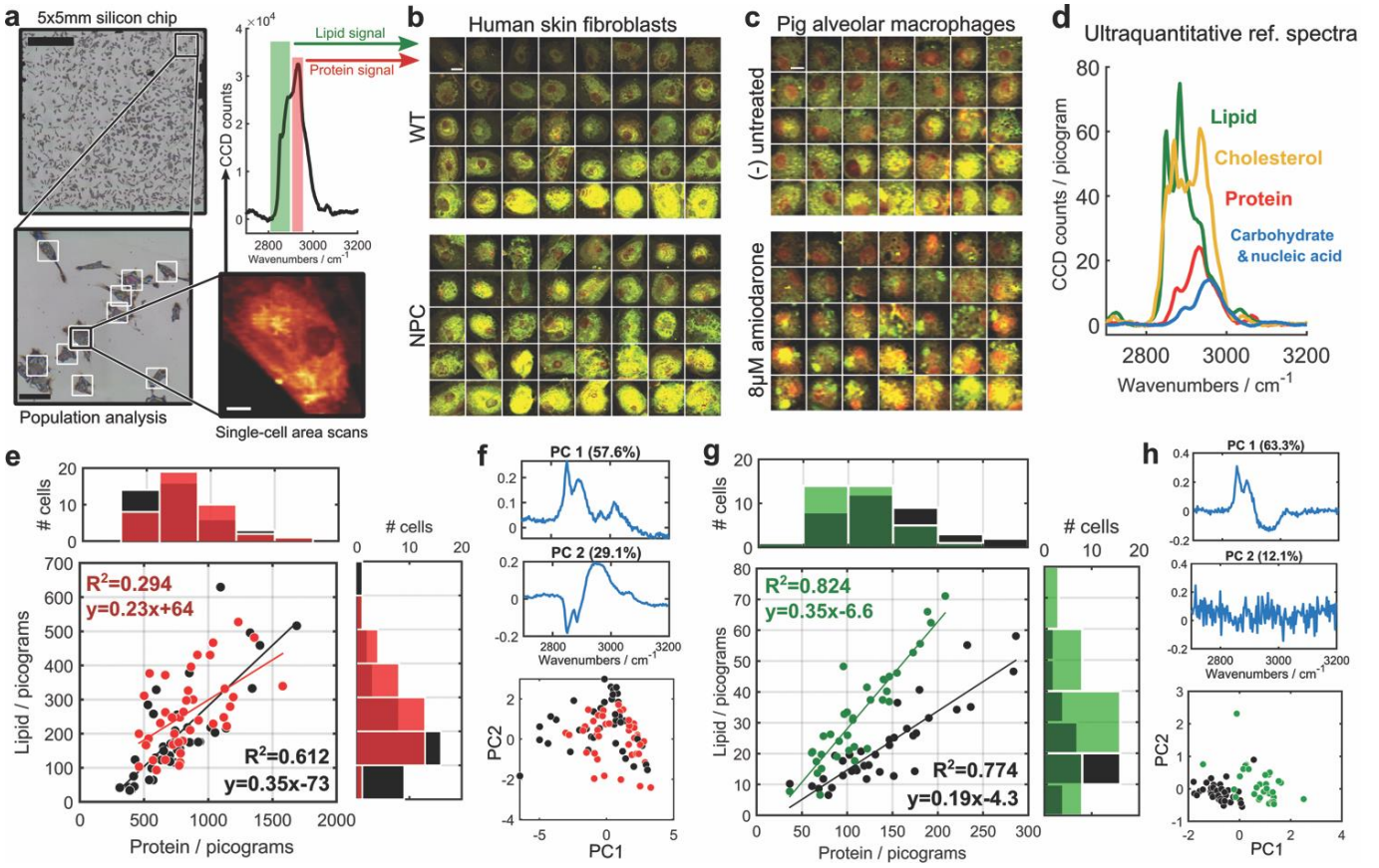

Figure 3. (a) Data acquisition and processing procedure; scale bars (from top-left to bottom-right): 1000μm, 100μm, and 10μm. Multi-band Raman images for (b) human skin fibroblasts (scale bar: 20μm) and (c) pig alveolar macrophages (scale bar: 10μm). (d) Reference spectra for linear combination modelling. (e) Single-cell compositional correlation plot and histograms showing fibroblast population distributions; each data point represents a single cell. WT in black, NPC in red. (f) First two PCA loading spectra and PCA score distribution plots (WT in black, NPC in red). (g) Single-cell compositional correlation plot and histograms showing alveolar macrophage population distributions; each data point represents a single cell. Untreated control group in black, drug-treated group in green. (h) First two PCA loading spectra and PCA score distribution plots (untreated in black, drug-treated in green).

composition measurements highlight the necessity of single-cell analyses, because cell population diversity and cell subpopulations are currently believed to play crucial roles in different disease states and have significant pathophysiological consequences. Although different cell types are expected to have different total mass contents, our reported picogram measurements are on the same order of magnitude as other reports of single-cell measurements in the literature.[20]

On average, there was a significant increase in total lipid content observed in the NPC cells relative to the WT group; 261.4±112pg compared to 195.6±140pg (mean±SD; p-value<0.05; t-test). The WT cell population exhibited a strong lipid-protein correlation (Pearson's coefficient, 0.782); NPC cells exhibited moderate correlation (Pearson's coefficient, 0.542), which was indicative of greater compositional heterogeneity on the single-cell basis (qualitatively verified by Raman images) and an uncoupling of the typical lipid-to-protein ratio. This presumably resulted from the compromised cholesterol transport and metabolism at the cellular level that is the hallmark of NPC disease (Figure 3e). Although cellular cholesterol measurements were not statistically-significant between WT and NPC, with respective values of 9.5±7.4 and 11.5±8.0 (mean ± SD; p-value>0.05; t-test), measurements were near our experimentally-determined limit of cholesterol quantitation (10pg in a 1000pg cell; or 1% wt/wt) and consistent with conventional methods of analysis, involving homogenization of cell populations and subsequent bulk measurements (normalizing the measured cholesterol content to the protein content of the entire population), yielding values in range of 5-20pg/cell.[4] For untreated and drug-treated macrophage populations, average lipid contents were 22.4±13.0pg/cell and 32.5±16.2pg/cell respectively, suggesting significant cellular lipid accumulation in response to amiodarone exposure (mean ± SD; p-value<0.05; t-test); these values are consistent with literature reports for amiodarone-induced phospholipidosis.[5] Lipid and protein were strongly correlated in untreated and drug-treated macrophages, with respective correlation coefficients of 0.880 and 0.908 (Figure 3g). Exposure to amiodarone induced a 1.5-fold increase in lipid-to-protein ratio per cell, evidenced by the increased slope of the drug-treated group's trend line. Logistic regression analysis revealed significant increases in lipid content and significant decreases in carbohydrate and nucleic acid content for the drug-treated cells compared to the untreated control cells (Figure S24, Table S1) but was unable to show significance for lipid increases in NPC group compared to WT with p-value=0.066 (Figure S25, Table S2). Principal component analysis (PCA) was performed on the same spectral datasets in parallel with ultraquantitation (Figure 3f, h); the first principal components (accounting for 57.6% of spectral variance in fibroblasts and 63.3% in macrophages) exhibited major peaks at 2850cm^{-1} and 2884cm^{-1} (the

characteristic Raman bands for C-H vibrations of lipids) and, as verified by our ultraquantitative results, were attributed to differences in cellular lipid content. K-means clustering of PCA results (Figure S26) could not differentiate WT and NPC fibroblasts, but discrimination of untreated and drug-treated alveolar macrophages yielded significant accuracy of 0.9143, sensitivity of 0.9714, and specificity of 0.8571 (p-value<0.05).

Conclusions

In conclusion, ultraquantitative single-cell Raman analysis enables more in-depth phenotypic characterization of cell populations than ever before possible with foreseeable application in basic research for the study of cellular accumulation phenomena, such as lysosomal storage disorders. The application of our mimic cell microarrays for quantitative calibration of single-cell measurements is not limited to Raman microscopy, as demonstrated herein; this technology could prove useful for quantitation in other single-cell techniques such as laser desorption and/or ionization mass spectrometry. The findings from this study represent a significant advancement in the cytometry field and open the doors of quantitative scientific perception to the entirety of the intracellular biomolecular matrix without artificial chemical tags, providing an approach by which scientists and clinicians may holistically explore the unadulterated biochemical realm within single cells: the building blocks of life.

Conflicts of interest

The authors declare the following competing interest(s): Dr. Gus R. Rosania is a consultant for Bristol-Myers Squibb.

Acknowledgements

Financial support of U.S. National Institutes of Health (R01GM078200 and R01GM127787 to GRR, R01NS063967 to APL, T32 GM007767 and T32 HL125242 to MVF, R01GM111400 to KAS), University of Michigan M-Cubed (to KAS, TJS, KR), Upjohn-Valteich award (to GRR), Ara Parseghian Medical Research Foundation (to APL and AS), University of Michigan Protein Folding Diseases Initiative (to APL and AS), American Foundation for Pharmaceutical Education (to MVF), DOD OCRP Early Career Investigator Award W81XWH-13-1-0134 (to GM), DOD Pilot award W81XWH-16-1-0426 (to GM). We thank Dr. Ki-Han Kim and the Office of Naval Research (ONR) for financial support under grant N00014-12-1-0874, Dr. Kenneth Caster and the Air Force Office of Scientific Research (AFOSR) for financial support under grant FA9550-10-1-0523, the National Science Foundation and Nanomanufacturing program for support through grant #1351412. We thank Dr. Pilar Herrero-Fierro and the Lurie Nanofabrication Facility for help with inkjet printing of calibration microarrays. We also thank Michigan Center for Integrative Research in Critical Care (MCIRCC), Dr. Kevin Ward, Dr. Hakam Tiba, Brendan McCracken, and Dr. Robert Dickson for help with the porcine experiments.

Author Contributions

VL, TJS, KR, KAS, and GRR conceived the study and aided in experimental design and discussions; VL, KAS, and GRR designed the ultraquantitative calibration theory; VL developed Raman analytical methods; VL and JM-M performed all Raman measurements; VL, MAM, and KS aided in Raman data statistical analyses; MVF, SYK, and AS synthesized and characterized HDL nanoparticles; CSS, GM, and AT performed atomic force microscopy analyses and contributed to engineering discussions of micro-calibration standard design; MVF, APL, and AS acquired and prepared human fibroblast samples; KAS facilitated porcine experimental model; VL performed macrophage drug incubation and preparation; VL wrote the manuscript with input from all authors; TJS, KR, APL, AS, KAS, and GRR contributed to scientific discussions regarding clinical relevance; KAS and GRR revised the manuscript and supervised the project.

Notes and references

1. Y. Yang, Y. Huang, J. Wu, N. Liu, J. Deng and T. Luan, *TrAC Trends in Analytical Chemistry*, 2017, **90**, 14-26.
2. C. A. Wassif, J. L. Cross, J. Iben, L. Sanchez-Pulido, A. Cougnoux, F. M. Platt, D. S. Ory, C. P. Ponting, J. E. Bailey-Wilson, L. G. Biesecker and F. D. Porter, *Genetics In Medicine*, 2015, **18**, 41.
3. L. Liscum, R. M. Ruggiero and J. R. Faust, *The Journal of Cell Biology*, 1989, **108**, 1625-1636.
4. C. Tängemo, D. Weber, S. Theiss, E. Mengel and H. Runz, *Journal of Lipid Research*, 2011, **52**, 813-825.
5. W. J. Martin and J. E. Standing, *Journal of Pharmacology and Experimental Therapeutics*, 1988, **244**, 774-779.
6. M. J. Reasor, C. L. Ogle, E. R. Walker and S. Kacew, *Am Rev Respir Dis*, 1988, **137**, 510-518.
7. G. J. Puppels, F. F. M. de Mul, C. Otto, J. Greve, M. Robert-Nicoud, D. J. Arndt-Jovin and T. M. Jovin, *Nature*, 1990, **347**, 301.
8. T. W. Bocklitz, S. Guo, O. Ryabchykov, N. Vogler and J. Popp, *Analytical Chemistry*, 2016, **88**, 133-151.
9. M. S. Bergholt, W. Zheng and Z. Huang, *Journal of Raman Spectroscopy*, 2012, **43**, 255-262.
10. M. S. Bergholt, W. Zheng, K. Lin, K. Y. Ho, M. Teh, K. G. Yeoh, J. B. Y. So and Z. Huang, *BIOMEDO*, 2011, **16**, 037003-037003-037010.
11. M. B. Albro, M. S. Bergholt, J. P. St-Pierre, A. Vinals Guitart, H. M. Zlotnick, E. G. Evita and M. M. Stevens, *npj Regenerative Medicine*, 2018, **3**, 3.
12. A. Y. F. You, M. S. Bergholt, J.-P. St-Pierre, W. Kit-Anan, I. J. Pence, A. H. Chester, M. H. Yacoub, S. Bertazzo and M. M. Stevens, *Science Advances*, 2017, **3**, e1701156.
13. X. Zhou, J. Dai, Y. Chen, G. Duan, Y. Liu, H. Zhang, H. Wu and G. Peng, *BIOMEDO*, 2016, **21**, 105002-105002.
14. A. Kuzmin, A. Pliss and P. Prasad, *Biosensors*, 2017, **7**, 52.
15. H. Wu, J. V. Volponi, A. E. Oliver, A. N. Parikh, B. A. Simmons and S. Singh, *Proceedings of the National Academy of Sciences*, 2011, **108**, 3809-3814.
16. V. LaLone, M. A. Mourão, T. J. Standiford, K. Raghavendran, K. Shedden, K. A. Stringer and G. R. Rosania, *Pharmaceutical Research*, 2018, **36**, 2.
17. M. K. Hammoud, H. K. Yosef, T. Lechtonen, K. Aljakouch, M. Schuler, W. Alsaidi, I. Daho, A. Maghnouj, S. Hahn, S. F. El-Mashtoly and K. Gerwert, *Scientific Reports*, 2018, **8**, 15278.
18. A. N. Kuzmin, S. M. Levchenko, A. Pliss, J. Qu and P. N. Prasad, *Scientific Reports*, 2017, **7**, 6512.
19. J. R. Mourant, K. W. Short, S. Carpenter, N. Kunapareddy, L. Coburn, T. M. Powers and J. P. Freyer, *BIOMEDO*, 2005, **10**, 031106-03110615.
20. J. R. Mourant, J. R. Dominguez, S. R. Carpenter, K. R. Short, T. R. Powers, R. Michalczyk, N. Kunapareddy, A. Guerra and J. P. Freyer, *Comparison of vibrational spectroscopy to biochemical and flow cytometry methods for analysis of the basic biochemical composition of mammalian cells*, SPIE, 2006.
21. A. Pliss, A. N. Kuzmin, A. V. Kachynski and P. N. Prasad, *Biophysical Journal*, 2010, **99**, 3483-3491.
22. A. Salehi-Reyhani, O. Ces and Y. Elani, *Experimental Biology and Medicine*, 2017, **242**, 1309-1317.
23. S. O. Konorov, H. G. Schulze, C. G. Atkins, J. M. Piret, S. A. Aparicio, R. F. Turner and M. W. Blades, *Analytical chemistry*, 2011, **83**, 6254-6258.

24. I. W. Schie, R. Kiselev, C. Krafft and J. Popp, *Analyst*, 2016, **141**, 6387-6395.
25. I. Barbulovic-Nad, M. Lucente, Y. Sun, M. Zhang, A. R. Wheeler and M. Bussmann, *Critical Reviews in Biotechnology*, 2006, **26**, 237-259.
26. P. Ihalainen, A. Määttänen and N. Sandler, *International Journal of Pharmaceutics*, 2015, **494**, 585-592.
27. R. Daly, T. S. Harrington, G. D. Martin and I. M. Hutchings, *International Journal of Pharmaceutics*, 2015, **494**, 554-567.
28. J. Sumerel, J. Lewis, A. Doraiswamy, L. F. Deravi, S. L. Sewell, A. E. Gerdon, D. W. Wright and R. J. Narayan, *Biotechnology Journal*, 2006, **1**, 976-987.
29. J. P. Segrest, R. L. Jackson, J. D. Morrisett and A. M. Gotto, *FEBS Letters*, 1974, **38**, 247-253.
30. J. Tang, D. Li, L. Drake, W. Yuan, S. Deschaine, E. E. Morin, R. Ackermann, K. Olsen, D. E. Smith and A. Schwendeman, *Journal of Lipid Research*, 2017, **58**, 124-136.
31. A. Schwendeman, D. O. Sviridov, W. Yuan, Y. Guo, E. E. Morin, Y. Yuan, J. Stonik, L. Freeman, A. Ossoli, S. Thacker, S. Killion, M. Pryor, Y. E. Chen, S. Turner and A. T. Remaley, *Journal of Lipid Research*, 2015, **56**, 1727-1737.
32. US6753313B1, 1997.
33. P. J. Blanche, E. L. Gong, T. M. Forte and A. V. Nichols, *Biochimica et Biophysica Acta (BBA) - Lipids and Lipid Metabolism*, 1981, **665**, 408-419.
34. B. A. Di Bartolo, S. J. Nicholls, S. Bao, K.-A. Rye, A. K. Heather, P. J. Barter and C. Bursill, *Atherosclerosis*, 2011, **217**, 395-400.
35. Y. Guo, W. Yuan, B. Yu, R. Kuai, W. Hu, E. E. Morin, M. T. Garcia-Barrio, J. Zhang, J. J. Moon, A. Schwendeman and Y. Eugene Chen, *EBioMedicine*, 2018, **28**, 225-233.
36. D. Li, M. V. Fawaz, E. E. Morin, R. Ming, D. Sviridov, J. Tang, R. Ackermann, K. Olsen, A. T. Remaley and A. Schwendeman, *Molecular Pharmaceutics*, 2018, **15**, 83-96.
37. T. H. BESSELING, J. JOSE and A. V. BLAADEREN, *Journal of Microscopy*, 2015, **257**, 142-150.
38. K. Galler, R. P. Requardt, U. Glaser, R. Markwart, T. Bocklitz, M. Bauer, J. Popp and U. Neugebauer, *Scientific reports*, 2016, **6**.
39. H. Jiang, M. K. Passarelli, P. M. Munro, M. R. Kilburn, A. West, C. T. Dollery, I. S. Gilmore and P. D. Rakowska, *Chemical Communications*, 2017, **53**, 1506-1509.
40. M. J. Reasor, C. L. Ogle and S. Kacew, *Toxicology and Applied Pharmacology*, 1989, **97**, 124-133.

Table of Contents Entry:

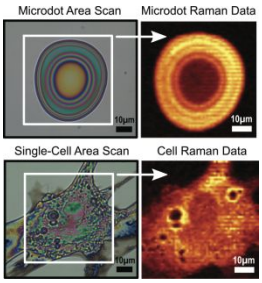

Micro-calibration standards containing picogram quantities of biomolecules were fabricated via inkjet printing, enabling quantitative analysis of single-cells via micro-Raman cytometry.